

Technical note

Improved analytical chip thickness model for milling

Lee M. Kumanchik*, Tony L. Schmitz

Department of Mechanical and Aerospace Engineering, University of Florida, Gainesville, FL, USA

Received 25 September 2006; accepted 6 December 2006

Available online 17 December 2006

Abstract

In this paper an analytic expression for chip thickness in milling was formulated while considering the cycloidal motion of the teeth, runout, and uneven teeth spacing. In order to generalize the equation, the cutting parameters associated with milling (linear feed, tool rotational speed, and radius) were combined into a single, non-dimensional parameter. The new parameter allowed abstraction of the milling process and enabled selection of the maximum possible chip thickness in milling. Equations for entry and exit angles of a cut were also developed. The chip thickness values given by the new model were compared to prior models and showed lower error levels.

© 2007 Elsevier Inc. All rights reserved.

Keywords: Tool path; Cycloid; Trochoid; Micro-milling

1. Introduction

Discrete part production by macro- and micro-milling remains an important manufacturing capability. To improve process efficiency and part quality, research efforts continue with a focus on pre-process performance predictions. Important aspects of milling models include developing an accurate description of the system dynamics and cutting forces; see [1] for an overview. The cutting forces are generally taken to be a function of the time varying chip thickness. Therefore, a number of authors have studied chip thickness in milling and reported various models [2–11].

In this work, we build on these previous studies to develop an analytical chip thickness model that incorporates the cycloidal trajectories of the cutter teeth, radial runout of individual teeth, and uneven teeth spacing. Expressions for entry and exit angles and limiting combinations of feed rate, spindle speed, and tool radius for chip formation are also provided. It is shown that: (1) the new model is more accurate than the well-known circular tooth path approximation and the analytical model presented in Ref. [12]; and (2) the accuracy does not degrade in the presence of runout. The reader may note that this is a geometric model only and does not incorporate such effects as minimum chip thickness and material elastic recovery observed in micro-milling [13].

2. Non-dimensional tool path

The path of the i th tooth in a milling cut can be described parametrically as

$$x_i = \rho\theta + r_i \sin(\theta + \phi_i), \quad y_i = r_i \cos(\theta + \phi_i), \quad (1)$$

where $\rho = f/\omega = N_t f_t / 2\pi$ is the radius of the circle that defines the cycloidal motion of the tooth, f the linear feed rate, ω the rotational speed of the tool, N_t the number of teeth on the tool, f_t the feed per tooth, r_i the radius of the i th tooth including runout, θ the instantaneous cutter angle, and ϕ_i is the angle between θ and the i th tooth. Fig. 1 shows a schematic of the tool path and tool. Eq.

* Corresponding author. Tel.: +1 352 392 8909; fax: +1 352 392 1071.
E-mail address: leemk@ufl.edu (L.M. Kumanchik).

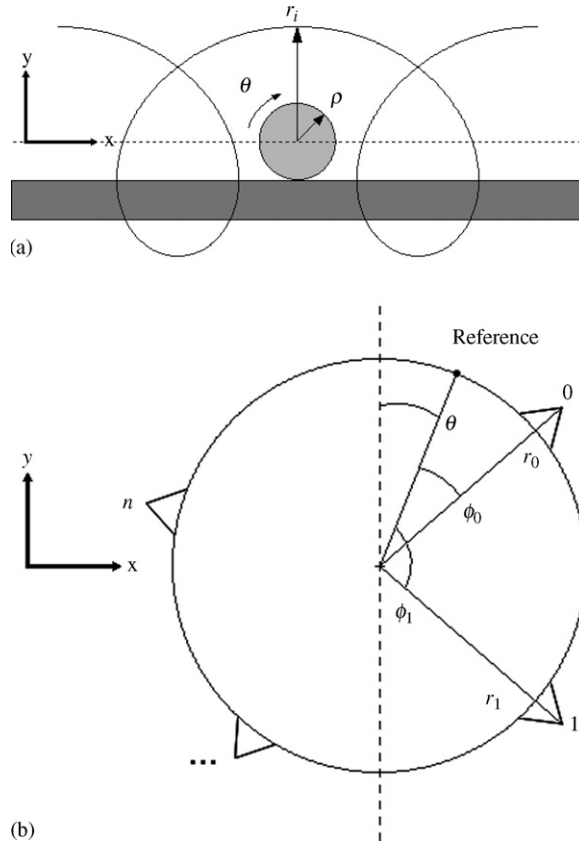


Fig. 1. (a) Path for a tooth of radius r_i attached to a circle of radius ρ which rolls along an imaginary surface. (b) A schematic of the milling tool. Teeth can be unevenly spaced and each tooth can have a different radius. The reference, θ , is common for all teeth; the difference in angular position for each tooth is the angle ϕ_i which is measured from the reference.

(1) can be rewritten in non-dimensional form by dividing by the nominal tool radius, r , yielding:

$$X_i = \frac{x_i}{r} = \varepsilon \theta + \alpha_i \sin(\theta + \phi_i), \quad Y_i = \frac{y_i}{r} = \alpha_i \cos(\theta + \phi_i), \quad (2)$$

where $\varepsilon = \rho/r$ is the non-dimensional cutting parameter, $\alpha_i = 1 + e_i$ the non-dimensional tool radius of the i th tooth which is nominally 1 but varies by e_i , and e_i is the runout of the i th tooth normalized with the nominal radius r . For no runout the non-dimensional path of any tooth is defined solely by ε . The non-dimensional parameter, ε , is proportional to the linear feed rate and inversely proportional to the rotational speed of the tool and the tool radius. As ε increases the tool path becomes more elongated and the chip thickness increases. Tool path plots for a two-tooth cutter with various ε values are provided in Fig. 2.

3. Limit of chip formation

The chip thickness in milling is defined as the distance between the current tooth's path and the previous tooth's path along the line segment connecting the tool center to the current tooth's cutting edge. Fig. 2c shows that for the given orientation the chip thickness definition is violated since the chip thickness is not defined between the current and previous paths and extends beyond the tool center. If the definition for chip thickness is to be satisfied, ε must be decreased so that the current tooth intersects the previous tooth's path as shown in Fig. 2b. The limit of chip formation is then given by the value ε_{lim} which forces all orientations of the current tooth between chip entry and exit to adhere to the definition for chip thickness. Though the orientations shown in Fig. 2 seem arbitrarily chosen, simulations show that this is the first orientation to violate the chip thickness definition as ε increases.

As a first approximation of the case shown in Fig. 2b, assume that the point of intersection, B, occurs on the line $Y=0$. Then at some point in time, t_0 , the leading tooth, $i+1$, rotates onto $Y_{i+1}=0$ at the angle $\theta_{t_0} + \phi_{i+1} = \pi/2$ and later in time, t_1 , the cutting tooth, i , rotates onto $Y_i = -\alpha_i$ at the angle $\theta_{t_1} + \phi_i = \pi$. For ε_{lim} these two locations share the same x -coordinate:

$$X_i(\theta_{t_1}) = X_{i+1}(\theta_{t_0}), \quad \varepsilon \theta_{t_1} + \alpha_i \sin(\theta_{t_1} + \phi_i) = \varepsilon \theta_{t_0} + \alpha_{i+1} \sin(\theta_{t_0} + \phi_{i+1}),$$

$$\varepsilon(\pi - \phi_i) + \alpha_i \sin(\pi) = \varepsilon \left(\frac{\pi}{2} - \phi_{i+1} \right) + \alpha_{i+1} \sin \left(\frac{\pi}{2} \right), \quad \varepsilon \left(\frac{\pi}{2} + \phi_{i+1} - \phi_i \right) = \alpha_{i+1}, \quad \varepsilon_{\text{lim}} = \frac{\alpha_{i+1}}{(\pi/2) + \phi_{i+1} - \phi_i}. \quad (3)$$

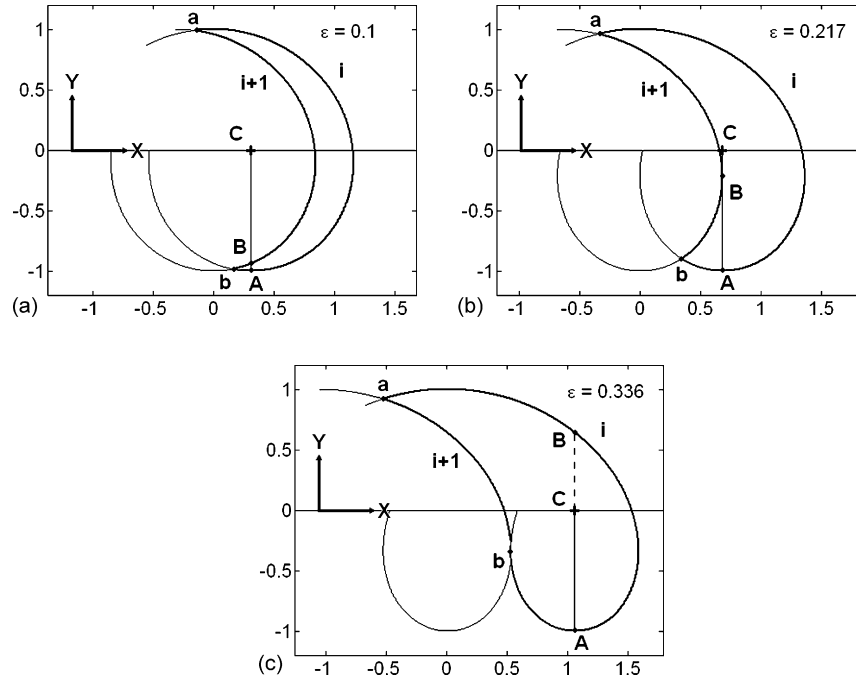


Fig. 2. Plots of the non-dimensional tool path with increasing ϵ values. Point A is the tip of the current tooth, i , B is the instantaneous intersection with the previous tooth's path, $i + 1$, and C is the tool center. The instantaneous chip thickness of the current tooth is the line segment AB. The outline of the chip being formed is highlighted using bold lines with (a) and (b) marking the tooth entrance and exit angles, respectively.

As shown by Eq. (3), the limiting ϵ value is a function of the angle difference between teeth and it increases for smaller teeth spacing. Evenly spaced teeth have the same angle difference between all teeth, $\phi_{i+1} - \phi_i = 2\pi/N_t$, but for unevenly spaced teeth the largest difference between any two consecutive teeth should be used for determining ϵ_{lim} . In addition, ϵ_{lim} is influenced by runout, therefore, the smallest tooth's non-dimensional radius should be used for the value of α_{i+1} when applying Eq. (3). Finally, if ϵ_{lim} is rewritten in familiar terms, $N_t f_i / 2\pi r$, and evenly spaced teeth are assumed, then $(f_i/r)_{lim} = 2\pi\alpha_{i+1} / (N_t(\pi/2 + \phi_{i+1} - \phi_i)) = \alpha_{i+1} / (N_t/4 + 1)$. It is important to note that even when written this way, $(f_i/r)_{lim}$ is still dependent on the number of teeth even though the quantity, f_i/r , is independent of the number of teeth.

In reality the true point of intersection, B, occurs when the tooth, $i + 1$, has an x -direction velocity of zero:

$$\frac{d(X_{i+1})}{d\theta} = \epsilon + \alpha_{i+1} \cos(\theta_{t_0} + \phi_{i+1}) = 0, \quad \theta_{t_0} + \phi_{i+1} = \arccos\left(-\frac{\epsilon}{\alpha_{i+1}}\right).$$

The next tooth, i , still rotates to $\theta_{t_1} + \phi_i = \pi$ and the x -coordinate of these two points are coincident:

$$\begin{aligned} X_i(\theta_{t+1}) &= X_{i+1}(\theta_t), & \epsilon\theta_{t+1} + \alpha_i \sin(\theta_{t+1} + \phi_i) &= \epsilon\theta_t + \alpha_{i+1} \sin(\theta_t + \phi_{i+1}), \\ \epsilon(\pi - \phi_i) + \alpha_i \sin(\pi) &= \epsilon \left[\arccos\left(-\frac{\epsilon}{\alpha_{i+1}}\right) - \phi_{i+1} \right] + \alpha_{i+1} \sin \left[\arccos\left(-\frac{\epsilon}{\alpha_{i+1}}\right) \right], \\ \epsilon \left[\pi - \arccos\left(-\frac{\epsilon}{\alpha_{i+1}}\right) + \phi_{i+1} - \phi_i \right] &= \alpha_{i+1} \sin \left[\arccos\left(-\frac{\epsilon}{\alpha_{i+1}}\right) \right], & \epsilon_{lim} &= \frac{\alpha_{i+1} \sin[\arccos(-\epsilon/\alpha_{i+1})]}{[\pi - \arccos(-\epsilon/\alpha_{i+1}) + \phi_{i+1} - \phi_i]}. \end{aligned} \quad (4)$$

Eq. (4) must be solved numerically for a given angle difference. A plot of Eqs. (3) and (4) versus angle difference, $\phi_{i+1} - \phi_i$, and the error between them, Δ_{er} , is provided in Fig. 3. The value of ϵ_{lim} is given for the angle difference corresponding to 2–5 tooth cutters with evenly spaced teeth. Most milling cuts have values of ϵ that are far below the limiting value, so ϵ_{lim} represents extremely aggressive cutting.

4. Analytical chip thickness

The uncut chip thickness of the current tooth is the distance between the current and previous tooth paths along the line segment connecting the tool center to the current tooth's cutting edge which is marked as AB in Fig. 2. The non-dimensional chip thickness

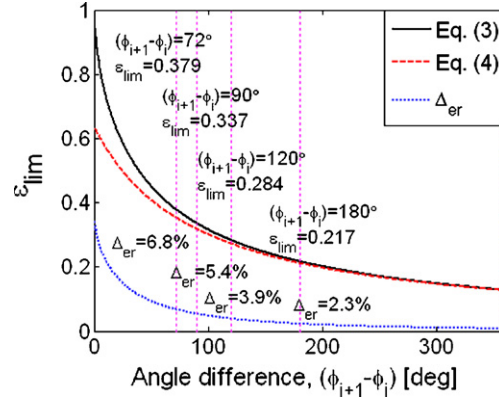


Fig. 3. Limiting value of ε to retain normal chip formation given the angle difference between successive teeth. Smaller angle differences enable more aggressive cutting.

is then

$$H_i = |AB| = |AC| - |BC| = \alpha_i - |BC|$$

$$H_i = \alpha_i - \sqrt{\left(X_{i+1}(\theta_0) - X_C(\theta_1)\right)^2 + \left(Y_{i+1}(\theta_0) - Y_C(\theta_1)\right)^2}$$

$$H_i = \alpha_i - \sqrt{\varepsilon^2 (\theta_0 - \theta_1)^2 + 2\varepsilon\alpha_{i+1} (\theta_0 - \theta_1) \sin(\theta_0 + \phi_{i+1}) + \alpha_{i+1}^2}, \quad (5)$$

where $|AC|$ and $|BC|$ are the distances between points A and C, and B and C, respectively, in Fig. 2, and X_C and Y_C are the coordinates of the tool center ($Y_C = 0$ always in the absence of tool vibrations which are not modeled here). As shown in [12], but rewritten in non-dimensional form, the relationship between θ_{t_0} and θ_{t_1} is

$$(\theta_{t_1} - \theta_{t_0})\varepsilon \cos(\theta_{t_1} + \phi_i) + \alpha_{i+1} \sin[(\theta_{t_1} + \phi_i) - (\theta_{t_0} + \phi_{i+1})] = 0. \quad (6)$$

In order to make Eq. (5) a function of the current cutting tooth's angle, θ_{t_1} , θ_{t_0} must be determined numerically from Eq. (6) [12]. However, the sinusoidal term in Eq. (6) contains the difference between the angle of the current cutting tooth, $\theta_{t_1} + \phi_i$, and leading tooth, $\theta_{t_0} + \phi_{i+1}$. Even for large ε values this difference is small, enabling a linear small angle approximation of the sinusoidal term ($\sin \theta = \theta$):

$$\begin{aligned} (\theta_{t_1} - \theta_{t_0})\varepsilon \cos(\theta_{t_1} + \phi_i) + \alpha_{i+1} \sin(\theta_{t_1} + \phi_i - \theta_{t_0} - \phi_{i+1}) &= 0, & (\theta_{t_1} - \theta_{t_0})\varepsilon \cos(\theta_{t_1} + \phi_i) + \alpha_{i+1}(\theta_{t_1} + \phi_i - \theta_{t_0} - \phi_{i+1}) &= 0, \\ \theta_{t_0}(\varepsilon \cos(\theta_{t_1} + \phi_i) + \alpha_{i+1}) &= \theta_{t_1} \varepsilon \cos(\theta_{t_1} + \phi_i) + \alpha_{i+1}(\theta_{t_1} + \phi_i - \phi_{i+1}), & \theta_{t_0} &= \frac{\theta_{t_1} \varepsilon \cos(\theta_{t_1} + \phi_i) + \alpha_{i+1}(\theta_{t_1} + \phi_i - \phi_{i+1})}{\varepsilon \cos(\theta_{t_1} + \phi_i) + \alpha_{i+1}}, \\ \theta_{t_0} &= \frac{\theta_{t_1}(\varepsilon \cos(\theta_{t_1} + \phi_i) + \alpha_{i+1}) + \alpha_{i+1}(\phi_i - \phi_{i+1})}{\varepsilon \cos(\theta_{t_1} + \phi_i) + \alpha_{i+1}}, & \theta_{t_0} &= \theta_{t_1} - \frac{\phi_{i+1} - \phi_i}{(\varepsilon/\alpha_{i+1}) \cos(\theta_{t_1} + \phi_i) + 1}. \end{aligned} \quad (7)$$

Substituting Eq. (7) into Eq. (5) yields the non-dimensional chip thickness for the milling operation expressed as a function of the non-dimensional parameter, ε , and the non-dimensional tool radius, α , in terms of the current cutting tooth angle, θ_{t_1} .

5. Entry and exit angles

The entry and exit angles for slotting (i.e., radial depth equal to the tool diameter) can be determined by setting Eq. (5) equal to zero:

$$\begin{aligned} H_i &= \alpha_i - \sqrt{\varepsilon^2(\theta_{t_0} - \theta_{t_1})^2 + 2\varepsilon\alpha_{i+1}(\theta_{t_0} - \theta_{t_1}) \sin(\theta_{t_0} + \phi_{i+1}) + \alpha_{i+1}^2} = 0, \\ \varepsilon^2(\theta_{t_0} - \theta_{t_1})^2 + 2\varepsilon\alpha_{i+1}(\theta_{t_0} - \theta_{t_1}) \sin(\theta_{t_0} + \phi_{i+1}) + \alpha_{i+1}^2 &= \alpha_i^2, \\ 2\varepsilon\alpha_{i+1}(\theta_{t_0} - \theta_{t_1}) \sin(\theta_{t_0} + \phi_{i+1}) &= \alpha_i^2 - \alpha_{i+1}^2 - \varepsilon^2(\theta_{t_0} - \theta_{t_1})^2, & \theta_{t_0} + \phi_{i+1} &= \arcsin \left[\frac{\alpha_i^2 - \alpha_{i+1}^2 - \varepsilon^2(\theta_{t_0} - \theta_{t_1})^2}{2\varepsilon\alpha_{i+1}(\theta_{t_0} - \theta_{t_1})} \right]. \end{aligned} \quad (8)$$

Since the entry and exit angles occur near $\theta + \phi = 0$ and $\theta + \phi = \pi$, respectively, Eq. (7) can be approximated as $(\theta_{t_0} - \theta_{t_1})_{\text{entry}} = (\phi_i - \phi_{i+1})/[(\varepsilon/\alpha_{i+1}) \cos(0) + 1]$ for the entry angle and $(\theta_{t_0} - \theta_{t_1})_{\text{exit}} = (\phi_i - \phi_{i+1})/[(\varepsilon/\alpha_{i+1}) \cos(\pi) + 1]$ for the exit angle. These results can then be substituted into Eq. (8):

$$\begin{aligned} (\theta_{t_0} + \phi_{i+1})_{\text{entry}} &= \arcsin \left[\frac{\alpha_i^2 - \alpha_{i+1}^2 - \varepsilon^2[(\phi_i - \phi_{i+1})/(\varepsilon/\alpha_{i+1} + 1)]^2}{2\varepsilon\alpha_{i+1}[(\phi_i - \phi_{i+1})/(\varepsilon/\alpha_{i+1} + 1)]} \right] \\ &= \arcsin \left[\frac{\varepsilon(-\phi_i + \phi_{i+1})}{2\alpha_{i+1}((\varepsilon/\alpha_{i+1}) + 1)} + \frac{(-\alpha_i^2 + \alpha_{i+1}^2)((\varepsilon/\alpha_{i+1}) + 1)}{2\varepsilon\alpha_{i+1}(-\phi_i + \phi_{i+1})} \right] \\ &= \arcsin \left[\frac{1}{2} \frac{\phi_{i+1} - \phi_i}{(\alpha_{i+1}/\varepsilon) + 1} + \frac{1 - (\alpha_i^2/\alpha_{i+1}^2)(\alpha_{i+1}/\varepsilon) + 1}{2} \frac{\phi_{i+1} - \phi_i}{\phi_{i+1} - \phi_i} \right], \end{aligned} \quad (9a)$$

$$(\theta_{t_0} + \phi_{i+1})_{\text{exit}} = \arcsin \left[\frac{1}{2} \frac{\phi_{i+1} - \phi_i}{(\alpha_{i+1}/\varepsilon) - 1} + \frac{1 - (\alpha_i^2/\alpha_{i+1}^2)(\alpha_{i+1}/\varepsilon) - 1}{2} \frac{\phi_{i+1} - \phi_i}{\phi_{i+1} - \phi_i} \right], \quad (9b)$$

Since the arcsine function in Eqs. (9a) and (9b) is multivalued, the expressions are not specific to any single chip being formed. However, if we consider the first chip to form, which has entry and exit angles near $(\theta_{t_0} + \phi_{i+1})_{\text{entry}} = 0$ and $(\theta_{t_0} + \phi_{i+1})_{\text{exit}} = \pi$, Eqs. (9a) and (9b) can be written using the principal inverse sine function:

$$(\theta_{t_0} + \phi_{i+1})_{\text{entry}} = \sin^{-1} \left[\frac{1}{2} \frac{\phi_{i+1} - \phi_i}{(\alpha_{i+1}/\varepsilon) + 1} + \frac{1 - (\alpha_i^2/\alpha_{i+1}^2)(\alpha_{i+1}/\varepsilon) + 1}{2} \frac{\phi_{i+1} - \phi_i}{\phi_{i+1} - \phi_i} \right], \quad (10a)$$

$$(\theta_{t_0} + \phi_{i+1})_{\text{exit}} = \pi - \sin^{-1} \left[\frac{1}{2} \frac{\phi_{i+1} - \phi_i}{(\alpha_{i+1}/\varepsilon) - 1} + \frac{1 - (\alpha_i^2/\alpha_{i+1}^2)(\alpha_{i+1}/\varepsilon) - 1}{2} \frac{\phi_{i+1} - \phi_i}{\phi_{i+1} - \phi_i} \right]. \quad (10b)$$

Eqs. (10a) and (10b) capture entry angles that fall between $[-\pi/2, \pi/2]$ and exit angles that fall between $[\pi/2, 3\pi/2]$, but they only define the angular position of the leading tooth, $i + 1$. If used together with Eq. (2), they can generate the angular position of the current cutting tooth, i , by setting the y -equations for the different teeth equal to each other and solving for $\theta_{t_1} + \phi_i$:

$$Y_i(\theta_{t_1}) = Y_{i+1}(\theta_{t_0}) \Rightarrow \alpha_i \cos(\theta_{t_1} + \phi_i) = \alpha_{i+1} \cos(\theta_{t_0} + \phi_{i+1}), \quad \theta_{t_1} + \phi_i = \arccos \left[\frac{\alpha_{i+1}}{\alpha_i} \cos(\theta_{t_0} + \phi_{i+1}) \right]. \quad (11)$$

Similar to before, the arccosine function in Eq. (11) is multivalued. The difference is that the principal inverse cosine function has an interval between $[0, \pi]$ and, depending on the system parameters, the entry and exit angles for tooth i can fall both inside and outside the interval. This means that Eq. (11) can assume four different forms when considering values near $(\theta_{t_1} + \phi_i)_{\text{entry}} = 0$ and $(\theta_{t_1} + \phi_i)_{\text{exit}} = \pi$:

$$(\theta_{t_1} + \phi_i)_{\text{entry}} = -\cos^{-1} \left\{ \frac{\alpha_{i+1}}{\alpha_i} \cos[(\theta_{t_0} + \phi_{i+1})_{\text{entry}}] \right\}, \quad (12a)$$

$$(\theta_{t_1} + \phi_i)_{\text{exit}} = 2\pi - \cos^{-1} \left\{ \frac{\alpha_{i+1}}{\alpha_i} \cos[(\theta_{t_0} + \phi_{i+1})_{\text{exit}}] \right\}, \quad (12b)$$

$$(\theta_{t_1} + \phi_i)_{\text{entry}} = \cos^{-1} \left\{ \frac{\alpha_{i+1}}{\alpha_i} \cos[(\theta_{t_0} + \phi_{i+1})_{\text{entry}}] \right\}, \quad (12c)$$

$$(\theta_{t_1} + \phi_i)_{\text{exit}} = \cos^{-1} \left\{ \frac{\alpha_{i+1}}{\alpha_i} \cos[(\theta_{t_0} + \phi_{i+1})_{\text{exit}}] \right\}. \quad (12d)$$

Eqs. (12a) and (12b) describe entry angles in the interval $[-\pi, 0]$ and exit angles in the interval $[\pi, 2\pi]$, while Eqs. (12c) and (12d) describe entry and exit angles in the interval $[0, \pi]$. Typically, Eqs. (12c) and (12d) are used when $(\alpha_{i+1}/\alpha_i) > 1$; however, all system parameters are important. In general, since the entry/exit angles come about from an intersection between the leading tooth, $i + 1$, and the current tooth, i , both sets of equations can be evaluated and the correct set determined by checking to see which generates an intersecting point using Eq. (2).

Table 1
Comparison between different feeds, spindle speeds, and diameters used to generate ε

Workpiece material	Spindle speed (rpm)	Feed (in./min)	Diameter (in.)	ε
Steel [14]	120,000	2.36	0.02	0.0003
Steel [12]	2,000	1.00	1/8	0.0013
Steel [12]	15,000	5.00	1/16	0.0017
Steel [14]	120,000	28.35	0.02	0.0038
Aluminum [12]	32,000	32.00	1/16	0.0051
Aluminum [12]	50,000	50.00	1/16	0.0051
Aluminum [12]	32,000	48.00	1/16	0.0076
Aluminum [12]	50,000	75.00	1/16	0.0076
Graphite [12]	15,000	30.00	1/16	0.0102
Graphite [12]	15,000	100.00	1/16	0.0340
Graphite [12]	15,000	70.00	0.02	0.0743
Graphite [12]	15,000	120.00	0.02	0.1273

The values were obtained from the references identified in the left column.

6. Results

In order to test the accuracy of the chip thickness equation developed here, comparison was made to other commonly used methods. The reference chip thickness was determined using the time domain simulation described in [8]; the reference was validated using the numerical solution in [13], referred to as (HLXL) in the subsequent examples. The analytical methods tested were: the solution provided here (Linear), the circular tooth path approximation (Circular), and the solution developed in [12] (WBIT).

Each method for calculating chip thickness was adapted in order to use the non-dimensional parameters described previously. Example ε values are listed in Table 1 to establish a baseline for comparison. The analytical chip thickness equations expressed in non-dimensional form are

$$H_i = \frac{2\pi}{N_t} \varepsilon \sin(\theta + \phi_i) \quad (\text{circular}), \quad H_i = \frac{2\pi}{N_t} \varepsilon \sin(\theta + \phi_i) - \frac{2\pi}{N_t} \varepsilon^2 \sin(\theta + \phi_i) \cos(\theta + \phi_i) + \frac{2\pi^2}{N_t^2} \varepsilon^2 \cos^2(\theta + \phi_i) \quad (\text{WBIT}).$$

A plot of the average error between each method and the reference for a two tooth slotting operation is provided in Fig. 4a. The value ε is varied from near zero to the limiting value for the selected case ($\varepsilon_{\text{lim}} = 0.217$). All analytical solutions deteriorate in their

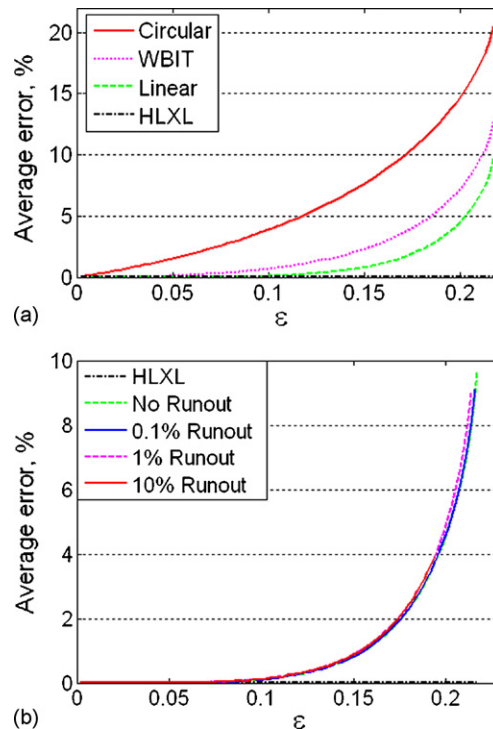


Fig. 4. (a) Average error with increasing values of ε for each solution as compared to the reference. (b) The error in the linear solution when runout is applied as compared to the reference with the same runout. In both cases, the HLXL solution shows $\sim 0\%$ error which verifies the reference.

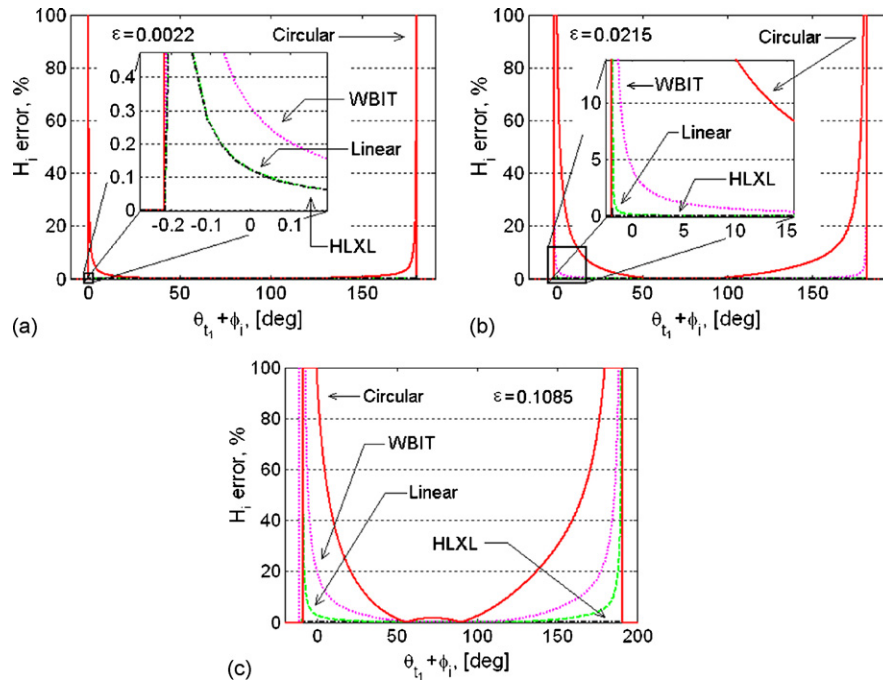


Fig. 5. The positive error in chip thickness as a function of cutter angle for a two tooth tool in a slotting cut. The error is capped at 100% and also is set to 100% if the solution being considered predicts a value for chip thickness when the time domain solution does not (the denominator of the error equation is zero). In (a) the linear solution has an error equal to the HLXL solution.

ability to predict average chip thickness as ϵ increases; however, the analytical solution described in this paper is more accurate than the other analytical solutions for every value of ϵ . The graph in Fig. 4b shows that if runout is included in the linear solution, its ability to predict chip thickness remains approximately the same. Fig. 5 shows the positive error in chip thickness between the time domain and the analytical solutions as a function of cutter angle for various ϵ values, again for two tooth slotting. The positive error has been capped at 100% to avoid distorting the graph when the value of the time domain simulation (the denominator of the error equation) is near or equal to zero.

7. Conclusions

In this paper an improved analytical model for chip thickness in milling was developed. First, the equations which describe tool motion were non-dimensionalized yielding two parameters that define the cutting conditions in milling. Using these parameters, the limit for chip formation was obtained. Then, the non-dimensional chip thickness was determined based on a small angle approximation of the sinusoidal term in the working equation. Finally, expressions for the entry and exit angles were provided. The method from this paper was then compared, along with other methods, to a time domain simulation. In all comparisons the method from this paper more closely approximated the time domain simulation than the other analytical approaches.

References

- [1] Smith S, Tlustý J. An overview of modeling and simulation of the milling process. *J Eng Ind Trans ASME* 1991;113:169–75.
- [2] Martellotti ME. An analysis of the milling process. *Trans ASME* 1941;63:677–700.
- [3] Martellotti ME. An analysis of the milling process. Part II. Down milling. *Trans ASME* 1945;67:233–51.
- [4] Sabberwal A. Chip section and cutting force during the milling operation. *Ann CIRP* 1961;10(1):197–203.
- [5] Tlustý J, MacNeil P. Dynamics of cutting forces in end milling. *Ann CIRP* 1975;24(1):21–5.
- [6] DeVor R, Kline W, Zdeblick W. A mechanistic model for the force system in end milling with application to machining airframe structures. In: Proceedings of the eighth NAMRC. 1980. p. 297–303.
- [7] Armarego E, Deshpande N. Computerized end-milling force predictions with cutting models allowing for eccentricity and cutter deflections. *Ann CIRP* 1991;40(1):25–9.
- [8] Schmitz T, Couey J, Marsh E, Tummond M. The role of cutter eccentricity on surface finish and milling forces. In: Proceedings of American society of mechanical engineers international mechanical engineering congress and exposition, IMECE2004-60232. 2004.
- [9] Montgomery D, Altintas Y. Mechanism of cutting force and surface generation in dynamic milling. *J Eng Ind Trans ASME* 1991;113:160–8.
- [10] Spiewak S. Analytical modeling of cutting point trajectories in milling. *J Eng Ind Trans ASME* 1994;116:440–8.
- [11] Spiewak S. Improved model of the chip thickness in milling. *Ann CIRP* 1995;44(1):39–42.

- [12] Bao WY, Tansel IN. Modeling micro-end-milling operations. Part I. Analytical cutting force model. Part II. Tool run-out. *Int J Mach Tools Manuf* 2000;40:2155–73, 2175–92.
- [13] Li HZ, Li XP. A numerical study of the effects of cutter runout on milling process geometry based on true tooth trajectory. *Int J Adv Manuf Technol* 2005;25:435–43.
- [14] Vogler M, Kapoor S, DeVor R. On the modeling and analysis of machining performance in micro-endmilling. Part I. Surface generation. Part II. Cutting force prediction. *J Manuf Sci Eng Trans ASME* 2004;126(4):685–94, 695–705.